Building and Environment 199 (2021) 107935

Contents lists available at ScienceDirect

Building and Environment

journal homepage: www.elsevier.com/locate/buildenv

Similarities and disparities in urban local heat islands responsive to regular-, stable-, and counter-urbanization: A case study of Guangzhou, China

Jiufeng Li [a], Wenfeng Zhan [a,b,*], Falu Hong [a], Jiameng Lai [a], Pan Dong [a], Zihan Liu [a], Chenguang Wang [a], Fan Huang [a], Long Li [a], Chunli Wang [a], Yingchun Fu [c], Shiqi Miao [a]

[a] Jiangsu Provincial Key Laboratory of Geographic Information Science and Technology, International Institute for Earth System Science, Nanjing University, Nanjing, Jiangsu, 210023, China
[b] Jiangsu Center for Collaborative Innovation in Geographical Information Resource Development and Application, Nanjing, 210023, China
[c] School of Geography, South China Normal University, Guangzhou, 510631, China

ARTICLE INFO

Keywords:
Surface urban heat island
Thermal remote sensing
Land surface temperature
Urbanization type
Urban renewal

ABSTRACT

Understanding the dynamics and spatial heterogeneity of the intra-city surface heat island (herein termed the surface urban heat island, SUHI) is critical for the design of urban heat mitigation strategies. Large disparities in the spatiotemporal variations of SUHIs are anticipated under different urbanization processes. However, most previous studies have focused solely on the inter-annual spatiotemporal SUHI variations of regular urbanization, while those for stable- and counter-urbanization remain largely unknown. Based on the remote identification of these three urbanization types over Guangzhou, China, we propose a novel strategy to investigate simultaneously the spatiotemporal variations and the associated controls of SUHIs. Our results indicate that: (1) Counter-, regular-, and stable-urbanization occurs mainly over the city center, city periphery, and the in-between areas, respectively. (2) The three urbanization types all demonstrate similar and significant growth in the daytime local SUHI intensity (SUHII). (3) There are significant disparities in the contributions of controls to the inter-annual daytime SUHII trends for these three urbanization processes. For the regular urbanization, the increase of the impervious surface percentage (ISP) dominates daytime SUHII growth, while the combination of ISP and residual factors (e.g., background climate and 3D urban geometry) leads for counter urbanization. For stable urbanization, the combination of residual controls and the increase in population density is the major factor. Urban divisional management may contribute to the mitigation of intra-city SUHI. Our findings potentially advance our understanding of changes in urban thermal environment under different urbanization processes.

1. Introduction

1.1. Background and objectives

Rapid urbanization causes dramatic changes in the urban environment [1,2]. One of these is the urban heat island (UHI) effect, a phenomenon in which the urban temperature is distinctly higher than that of the rural surroundings [3,4]. With the intensification of the UHI effect and its negative impacts on human health, along with rapid urbanization [5], the investigation of the UHI and its controls has become a focus of urban climate studies [6]. Some of the studies have used *in-situ* or vehicle-based temperature measurements to monitor UHI, yet such measurements can only provide limited and sparse spatial coverage [7,8]. Satellite-based land surface temperature (LST) provides a more spatially detailed view of the surface UHI (SUHI) via spatially continuous and temporally-repeated observations [9,10]. In recent years there has been an increasing number of studies that use satellite-derived LSTs for SUHI investigations [4], as well as for urban planning and management [11].

There are two main strands of SUHI studies: the first focuses on the comparison of SUHI variations among a great number of cities distributed within an extensive region [12–15], while the second focuses on changes in intra-city SUHI within individual cities [16–20]. Within an extensive region, cities across countries and climates are characterized

* Corresponding author. Nanjing University at Xianlin Campus, No.163 Xianlin Avenue, Qixia District, Nanjing, Jiangsu, 210023, PR China.
E-mail address: zhanwenfeng@nju.edu.cn (W. Zhan).

https://doi.org/10.1016/j.buildenv.2021.107935
Received 20 January 2021; Received in revised form 5 April 2021; Accepted 29 April 2021
Available online 1 May 2021

by significant inter-city SUHI variations. Such variations are determined by various controls, such as urban land cover, anthropogenic heat release (AHR), rural background, and background climate [12–15, 21–24]. For individual cities, they have experienced different urbanization processes, including regular- (urban expansion), stable-, and counter-urbanization under diverse phases of the development of urban economy and the long-term impact of urban planning [25,26]. These different urbanization processes lead to a large heterogeneity in local SUHI [27–33], even within a single city. There is usually a significant temporal disparity of the local SUHI over surfaces that experience different types of urbanization [22,23,34].

The major objective of this study is to investigate the local SUHI and the associated controls responsive to different urbanization processes, using Guangzhou (a megacity in China) as a case study. The specific objectives of this study are as follows: (1) to identify urban surfaces that have experienced the three urbanization processes; (2) to examine and compare the inter-annual SUHI variations responsive to these processes; and (3) to separate the contribution of each control that results in the observed SUHI variations.

The following contents of this paper are organized as follows. Section 1.2 provides a literature review on the remote sensing of different types of urbanization as well as the associated impacts on local SUHIs. Section 2 introduces the study area and the used data (Section 2), which are then followed by the presentation of the methodology for the estimation of the local SUHIs over surfaces that undergo different types of urbanization as well as for the quantification of the contributions from the associated controls (Section 3). Sections 4 and 5 display the results and implications of this study, respectively. The conclusions are finally drawn in Section 6.

1.2. Literature review on different types of urbanization and their impacts on local SUHIs

With regular urban growth especially in developing countries, currently regular urbanization, characterized by a continuous increase in the impervious surface density, is receiving wide attention [35–37]. The inter-annual SUHI variations responsive to regular urbanization are mainly modulated by four controls: (1) The impervious surface percentage (ISP): Over newly-urbanized areas, both the daytime and nighttime SUHI intensity (SUHII) usually increases as natural surfaces are transformed into urban impervious land [7,10]. Like the case of newly-urbanized areas, the nighttime SUHII can also increase because of urban densification over urban cores (typified by an increase in ISP and a decrease in the sky view factor) [38]. Unlike the situation at night, along with urban densification over urban cores, the daytime SUHII may increase due to decreased evaporative cooling with a higher ISP; and it may also decrease due to a more significant shading effect among tall buildings [10,30]. (2) AHR: Along with urban expansion or densification, both the daytime and nighttime SUHII can be strengthened by the increased AHR generated by rising energy consumption [39,40]. (3) Rural background: The daytime SUHII is anticipated to increase with the cooling of the rural background, which is caused by increased vegetation evapotranspiration [13,22,34] as the rural background continues to become greener [14,41], although the nighttime SUHII is less impacted by the rural background greening. (4) Background climate: The daytime SUHII can either be enhanced or weakened in different background climate [24], but the former scenario is expected to occur more frequently as the warming of the background climate usually magnifies the urban-rural contrast in LST [23,24].

Differing from regular urbanization that usually occurs around city peripheries, stable urbanization mostly emerges over already-urbanized surfaces where there have been few new urban constructions (e.g., buildings and roads) for periods [25,26,42]. Stable urbanization is usually characterized by minor or even no change in impervious surface density [25,26]. Compared with the numerous studies focusing on regular urbanization, relatively few investigations have examined the inter-annual SUHI variations of stable urbanization. Previous studies have demonstrated that the SUHII over stable-urbanization surfaces also shows a rising trend, but with a different rate of increase compared to that over regular-urbanization surfaces [23,34]. In terms of controls, the cooling of the rural background has been shown to contribute to the increase in SUHII over stable-urbanization surfaces [34]. It is anticipated that the disparate behavior in impervious surface density and AHR over stable-urbanization surfaces [22], as well as background climate change, can play a role [43,44]. Nevertheless, the individual contributions of these controls to inter-annual SUHI variations over stable-urbanization surfaces remain considerably unclear.

With urban renewal, especially over old urban areas, counter urbanization (or urban renewal) occurs in some city cores [25,26,45,46]. Counter-urbanization surfaces are characterized by a decrease in impervious surface density. Although receiving less attention compared with the other two urbanization processes, counter urbanization fills the gap in understanding renewal-related changes in city cores. Recent studies have shown that renewal-related counter urbanization is observable in large cities, such as Guangzhou and Shanghai in China, and Lyon in France, by remote sensing [20,25,46]. Counter urbanization (or urban renewal) can lead to a reduced SUHII because the LST of city core can decrease with the decline in impervious surface density [20, 47]. Compared with regular- and stable-urbanization, the controls on counter urbanization should differ, given that such an urbanization process is often accompanied by a decrease in impervious surface density and AHR [46,48]. However, like those of stable urbanization, the inter-annual SUHI variations and the associated controls for counter urbanization remain poorly understood.

Despite the progress made in SUHI investigations from the perspective of urbanization type, especially those for regular-urbanization surfaces, several issues remain to be addressed. First, the inter-annual SUHI variations for those surfaces with stable- and counter-urbanization remain largely unknown. Second, the contributions from various controls to inter-annual SUHI variations responsive to these three urbanization processes have not yet been comprehensively evaluated and consequently are also unclear. This *status quo* has hindered our in-depth understanding of inter-annual SUHI variations under these three different urbanization processes.

2. Study area and data

2.1. Study area

Guangzhou (22°26′-23°56′N, 112°57′-114°03′E), the study area, is the provincial capital city of Guangdong Province and a national central city in China (Fig. 1). It is located within the subtropical climate zone where the surfaces are covered mainly by evergreen broadleaved forest; the annual mean precipitation and temperature are 1,800 mm and 22.7 °C, respectively. The population in Guangzhou is 14.9 million (2018), and its urbanization rate is higher than 86%, which is significantly larger than the mean level of China [49]. In the past three decades, Guangzhou has experienced considerable expansion – its impervious surfaces, mostly of medium- and high-density, have increased by around eight times [50]. Since 2000, the city administration has produced a series of urban planning strategies to renew old urban areas, including the ‘Short-term Construction Plan of Guangzhou (2002–2005)’, the ‘Special Eleventh Five-year Plan of Guangzhou (2006–2010)’ (http://www.gz.gov.cn/zwgk/ghjh/zxgh/content/mpost_2837440.html), and the ‘Three Old Renewals of Guangzhou (2011–2015)’ [51]. With these multiple urban planning strategies, different urbanization processes, such as regular-, stable-, and counter-urbanization, have developed simultaneously in Guangzhou and made it a valuable case.

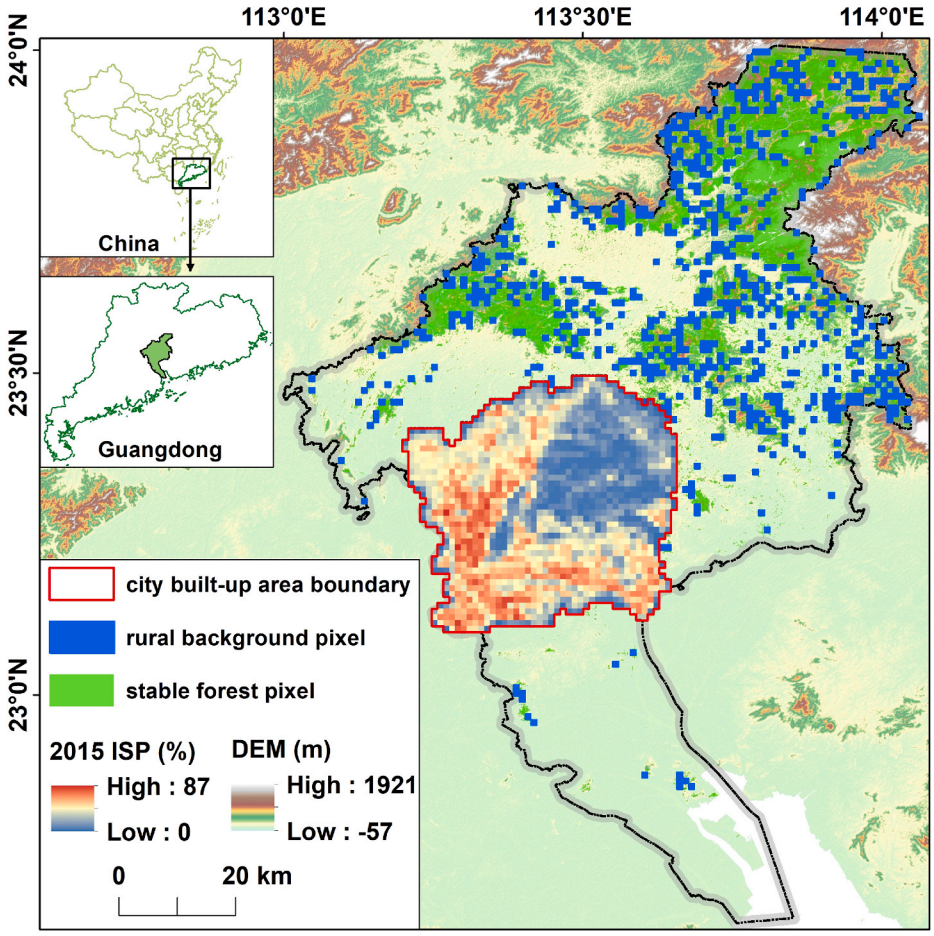

Fig. 1. Geolocation of Guangzhou city. The colors within the red polygon (the boundary of the city built-up area) denote the impervious surface percentage (ISP, 2015); the green dots denote forest pixels stable for a long duration; and the blue pixels are the defined rural background extracted from the green dots but with DEM < 100 m. (For interpretation of the references to color in this figure legend, the reader is referred to the Web version of this article.)

2.2. Data

2.2.1. MODIS products

The MYD11A1 product from 2003 to 2015 (downloaded from https://ladsweb.modaps.eosdis.nasa.gov/) was used to analyze inter-annual SUHI variations under different urbanization processes. This product includes daily LSTs acquired at 13:30 and 1:30 local time, with a spatial resolution of 1 km. The daily LSTs were further composited into seasonal mean values through simple temporal aggregation with the null values excluded. Note that we only used the summer data (from June to August) because urban residents are exposed to higher heat stress during this season [12,52]. The MYD13A3 product from 2003 to 2015 was further used to extract monthly mean enhanced vegetation index (EVI) data, also with a spatial resolution of 1 km and with simple temporal aggregation. These EVI data were used analyze vegetation changes in the rural background.

2.2.2. Impervious surface data

The impervious surface percentage (ISP) data (2003–2015) derived from Ref. [25], with an overall accuracy of 84%, were used to identify the surfaces that experienced different urbanization processes. These data were generated based on the inter-annual optimized Cubist tree model with a spatial resolution of 30 m [25,53]. These 30-m ISP data were further resampled to 1 km to match the spatial resolution of the LST and EVI data.

2.2.3. Auxiliary data

(*i*) Land use data. The land use data were derived from Ref. [54] using the Continuous Change Detection and Classification (CCDC) algorithm; and they are able to satisfy the requirement of this research with an overall accuracy of 87.05% [55,56]. With the land use data, we retrieved the stable forested areas that are adjacent to the city boundary of Guangzhou (green dots in Fig. 1). These stable forested areas have been stable for years and therefore suitable to be used for determining the rural background required for the SUHII calculation [57]. (*ii*) The population density (https://landscan.ornl.gov/landscan-datasets) [58] and digital elevation model (DEM) data (https://topotools.cr.usgs.gov/gmted_viewer/viewer.htm). The former and latter were used to help delineate the AHR and rural background, respectively; and they were also resampled to 1 km to match the spatial resolution of the LST data.

3. Methodology

Three steps were used to investigate inter-annual SUHI variations and their controls for surfaces with regular-, stable-, and counter-urbanization (Fig. 2). First, we delineated the rural background by combining the land cover type and DEM data (Section 3.1.1). The urban surfaces that experienced these three urbanization processes were then identified by analyzing both the ISP changes and the associated significance level (p-value) during the study period (Section 3.1.2). Second, we calculated both the pixel-based and overall SUHI intensities of the three urbanization types, based on which the inter-annual SUHI variations were examined (Section 3.2). Finally, we separated the individual

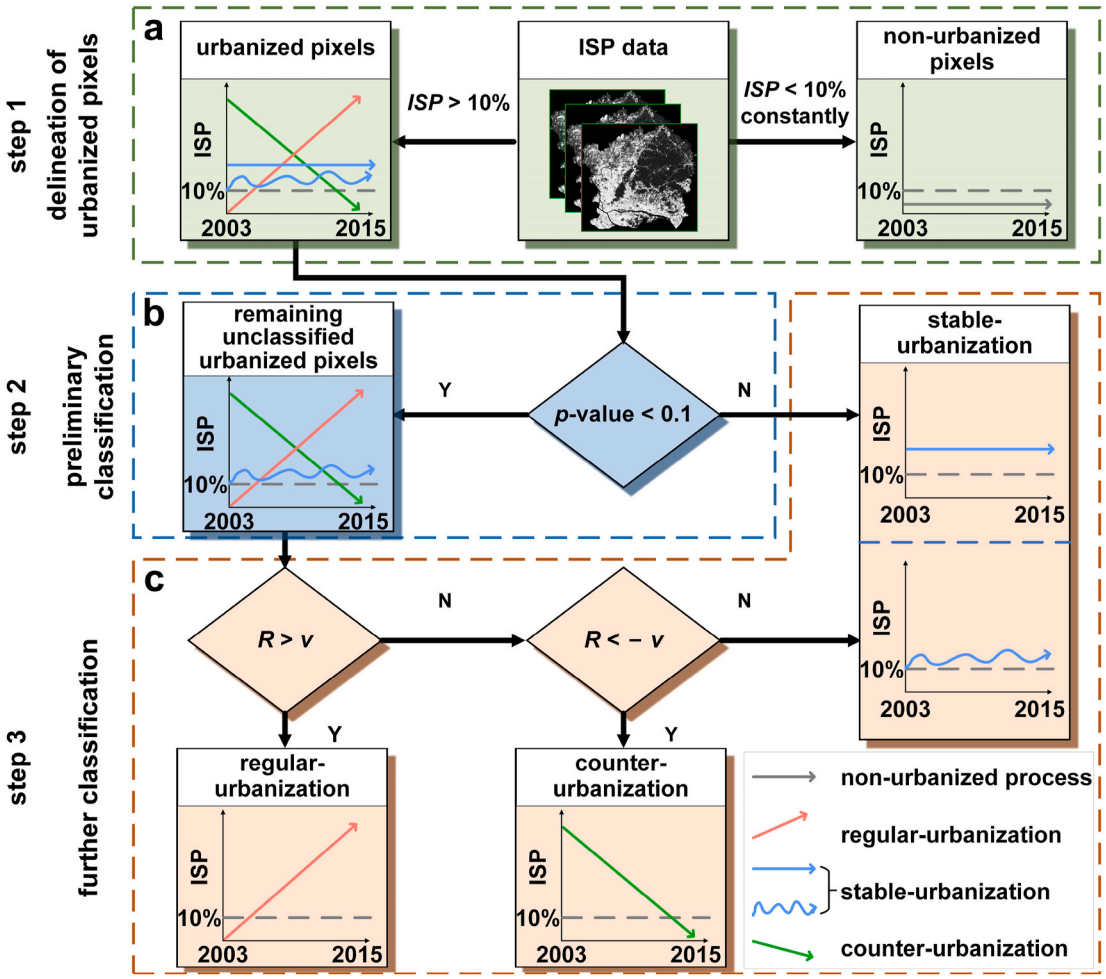

Fig. 2. Flowchart for the identification of surfaces that experienced three different types of urbanization process. ISP is the impervious surface percentage; R is the relative change rate given in Eq. (1); and v is the vertex of the histogram for R.

contributions from different controls to the SUHI variations (Section 3.3).

3.1. Identification of the rural background and surfaces with different urbanization processes

3.1.1. Identification of the rural background

The rural background was defined as forested land adjacent to the urban areas of Guangzhou (green dots in Fig. 1) [57]. These forests are rarely affected by urbanization and they remained relatively stable during the study period. Furthermore, the pixels with elevations exceeding 100 m of the mean elevation of the rural background (blue dots in Fig. 1) were removed to reduce the impact of altitude on the estimation of SUHII.

3.1.2. Identification of surfaces undergoing different urbanization processes

Impervious surface percentage (ISP) is one of the most important indictors responding to the changes in urbanization [1]. Within the urban areas, we first designated the pixels with very low ISP (<10%) during the entire study period as non-urbanized surfaces, and then obtained the urbanized pixels by excluding the non-urbanized pixels (see Step 1 in Fig. 2a). Among the urbanized pixels, stable urbanization surfaces were identified by determining the significance level of the ISP trend (Step 2 in Fig. 2b). The remaining unclassified urbanized pixels were further separated into regular- and counter-urbanization surfaces by analyzing the magnitude of ISP change (Step 3 in Fig. 2c). Note that the detailed steps of these identifications are provided in Note S1 in Supplementary Material.

Step 1. *Delineation of urbanized pixels*. To better reflect the impact of urbanization on the SUHI, the pixels with ISP <10% during the entire study period were first excluded prior to subsequent identification [25]. These pixels were designated as non-urbanized pixels while the rest were designated as urbanized pixels.

Step 2. *Preliminary classification of urbanized pixels*. The urbanized pixels were divided into two groups by diagnosing the significance level of the ISP trend using ordinary least square regression analysis (OLS). The OLS was used to calculate the p-value of the ISP trend over urban pixels. The p-value is a necessary requirement for identifying whether urban pixels have undergone significant changes. The first group includes the stable-urbanization surfaces which lack a significant ISP trend, while the second includes the remaining unclassified urbanized pixels that have a significant ISP trend. The retrieval of the ISP can be considerably impacted by cloud contamination [59], which may reduce the significance level of the ISP trend and affect the identification of true urban changes [36]. Therefore, the threshold of the significance level was set as 0.1 ($p < 0.1$) rather than to lower values such as 0.05 [53], to preserve as many as possible of the urbanized pixels that had undergone true changes. The pixels with $p > 0.1$ were labelled as stable urbanization surfaces while the other pixels with $p < 0.1$ were labelled as remaining unclassified urbanized pixels that require further identification (see Step 3).

Step 3. *Further classification of the remaining unclassified urbanized pixels*. The remaining unclassified urbanized pixels do not completely correspond to the regular- and counter-urbanization surfaces since they may still include several stable- urbanization pixels. This is because small ISP changes and false ISP changes due to retrieval errors are unable to reflect true urban changes [36]. Therefore, these remaining urbanized pixels were further divided by the relative change rate of the ISP [60], using the following formula:

$$R = \frac{s_e - s_s}{s_s} \times 100\% \quad (1)$$

Here, R is the relative change rate of the ISP; s_e and s_s are the ISP values fitted using the OLS at the end and start year of the study period for each pixel, respectively.

The R value of each remaining unclassified urbanized pixel was calculated using Eq. (1), and the histogram of the absolute value of R was also generated (Fig. 3b). Using the vertex (i.e., v) of the R histogram as the boundary, the remaining unclassified urbanized pixels were divided into two groups [36]: Those with absolute R less than v (i.e., $-v < R < v$) were grouped into stable urbanization surfaces, whereas those with absolute R greater than v (i.e., $R > v$) and with absolute R lower than $-v$ (i.e., $R < -v$) were defined as regular- and counter-urbanization surfaces, respectively.

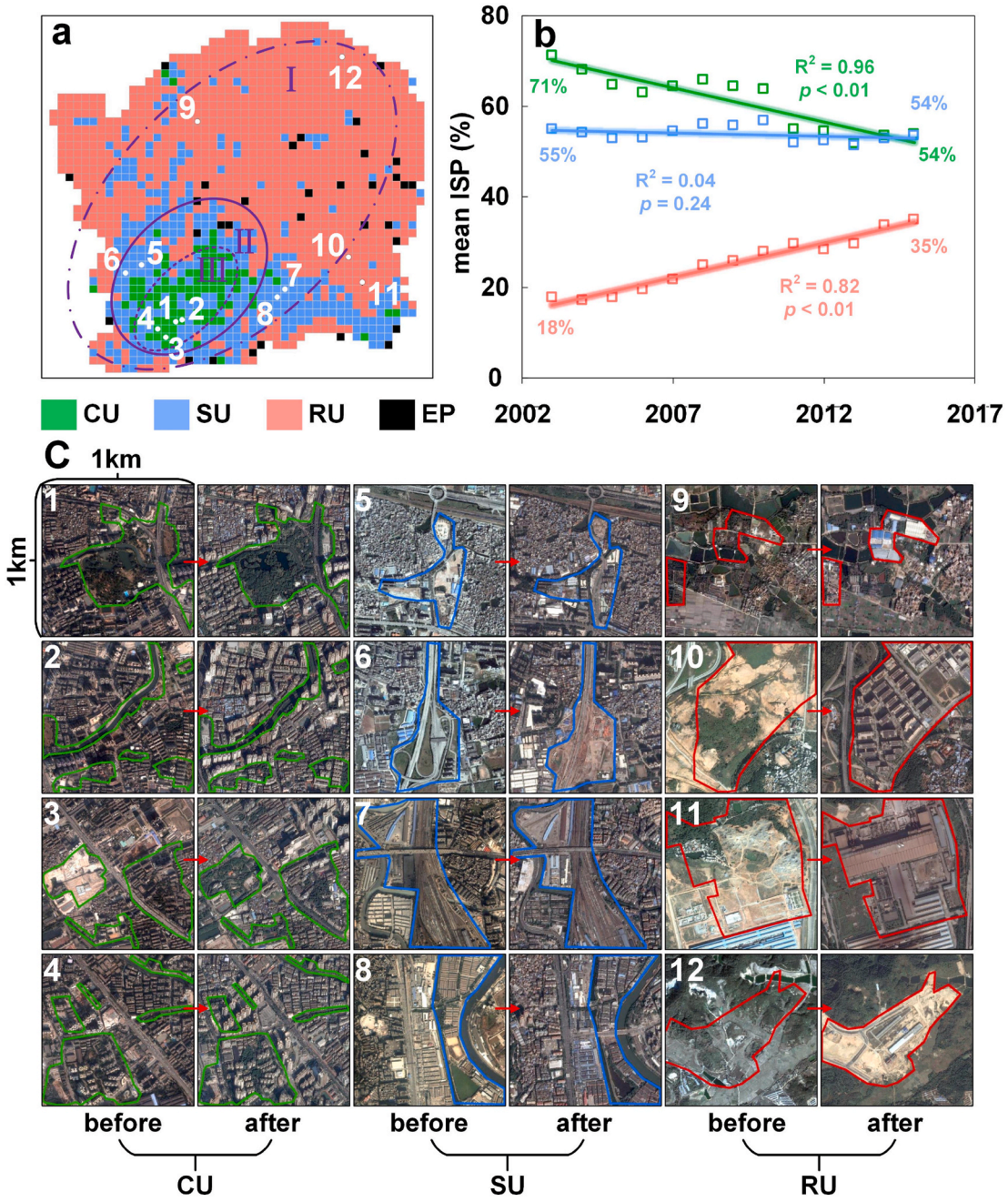

Fig. 3. Spatial distribution (**a**) and annual mean ISP variations (**b**) of regular urbanization (RU), stable urbanization (SU), and counter urbanization (CU). EP denotes the 'erased pixel'; Ellipses I, II, and III in (**a**) denote the approximate areas formed by regular-, stable- and counter-urbanization pixels, respectively; and the numbers '1' to '12' in (**a**) represent the pixel location of 12 pairs of high-resolution Google Earth images (**c**) which denote the surface status before and after the associated urbanization process.

3.2. Calculation of the SUHII of surfaces with different urbanization processes

The pixel-based SUHII was calculated as the LST difference between each urbanized pixel (including all three urbanization types) and the rural background, given as follows:

$$I_u = T_u - T_{r\_m} \quad (2)$$

where T_u is the LST for each urbanized pixel, and T_{r_m} is the mean LST of rural background. Furthermore, the overall SUHII for each urbanization type was obtained by further averaging the SUHIIs for all pixels from each urbanization type.

3.3. Separation of contributions from different controls

Inter-annual SUHII variations are regulated primarily by controls such as urban land cover status, AHR, rural background, background climate, and changes in city size [21–24,43,61]. We used the ISP to quantify the contribution of the urban land cover status to inter-annual SUHII variations, mainly because the ISP is a key surface parameter of urban land cover status and has been widely used for this purpose [7, 24]. We used population density (POD) as a proxy for quantifying the AHR-induced contribution [39], and the rural background LST (RBL) for reflecting the contribution from the rural background [23], as it is directly involved in the SUHII calculation (see Eq. (2)). It is very difficult to calculate the contributions from the rest factors such as changes in the background climate, city size, economic activities, and transportation systems, as well as those from the interactions among the controls. We therefore combined all such residual factors (REF) as a single control and estimated their contributions using the residual method [62]. We acknowledge that several other physical factors (e.g., the economic activities and transportation systems) can also be used to represent urban land cover status [24,30,63], and most of them can be characterized by remotely-sensed surface parameters, such as vegetation, nighttime light data, and urban 3D geometry. Nevertheless, these surface factors are either closely related to the ISP and population density (such as the NDVI and nighttime light data), or are relatively difficult to obtain at the city scale (urban 3D geometry).

The separated contributions from these controls to inter-annual SUHII variations satisfy the following formula [62]:

$$K_u = K_s + K_p + K_r + K_o \quad (3)$$

where K_u is the observed inter-annual SUHII change rate; and K_s, K_p, K_r, and K_o are the inter-annual SUHII change rates induced by ISP, POD, RBL, and REF respectively. These parameters were calculated using the following strategies: (1) K_u was directly calculated as the observed change rate of SUHII for each urbanization type using Eq. (2). (2) K_s was estimated as the SUHII change rate induced by ISP. Nevertheless, it is difficult to separate the ISP-induced contribution from a temporal perspective because the SUHII dynamics is controlled by a series of controls in addition to the ISP [64], although this parameter is closely related to inter-annual SUHII variations [7]. To address this, we derived the relationship between ISP and SUHII using the 'space-for-time substitution' strategy [65,66]. In other words, we first established the general statistical relationship between the ISP and SUHII from the spatial perspective (i.e., by combining different pixels), and then used the relationship to quantify the individual ISP-induced contribution to inter-annual SUHII variations. (3) K_p was estimated as the inter-annual SUHII change rate induced by POD. POD has also been shown to be well correlated with inter-annual SUHII variations [67,68]. However, similar to ISP, it is difficult to separate the POD-induced contribution from the temporal perspective. Therefore, we again used the 'space-for-time substitution' strategy to derive the relationship between POD and SUHII variations. (4) K_r was estimated as the SUHII change rate induced by RBL. The calculation of SUHII is directly impacted by RBL (see Eq. (2)). The RBL-induced contribution is equivalent to its own change rate and was thus quantified as the observed increment of the annual mean rural background LST referenced to the annual mean of the starting year of the study period. (5) K_o was calculated as K_u minus the sum of addition of K_s, K_p, and K_r. We are aware of that there may be uncertainties in the 'space-for-time substitution' strategy for estimating the ISP- and POD-induced contributions, as well as in approach for estimating the REF-induced contribution. Further discussion of these issues is given in Section 5.2.

The foregoing analysis shows that K_u can be directly calculated using the LST observations, and that K_o can be quantified once K_s, K_p, and K_r are available. K_s, K_p, and K_r can be calculated using the following equations:

$$\begin{cases} K_s = Trend[\lambda_s \cdot m_s(t)] \\ K_p = Trend[\lambda_p \cdot m_p(t)] \\ K_r = Trend[T_{r\_s} - T_{r\_m}(t)] \end{cases} \quad (4)$$

Here $Trend[\cdot]$ denotes the function used to derive the linear trend of SUHII of each control with time (K·decade^{-1}); λ_s and λ_p are the linear regression slopes between ISP (or POD) and the observed SUHII obtained using the 'space-for-time substitution' strategy, respectively; $m_s(t)$ and $m_p(t)$ are the annual mean ISP and POD in year t, respectively; T_{r_s} is the rural background LST at the start year of the study period; and T_{r_m} is the annual mean rural background LST in year t.

4. Results

4.1. Spatial distribution of different urbanization types

The spatial distribution and the annual mean ISP changes for the regular-, stable-, and counter-urbanization surfaces are presented in Fig. 3, with the identification details given in Note S1 in Supplementary Material. In terms of spatial distribution, these three types of urbanization surface show a spatial structure of concentric ellipses from the interior to the exterior, with Ellipses I, II, and III representing the regular-, stable-, and counter-urbanization surfaces, respectively (Fig. 3a).

In terms of urbanization type, regular-urbanization surfaces account for the largest area (62%) and they are mostly located in the city periphery (Ellipse I, the northeastern region, as shown in Fig. 3a). During the study period, the annual mean ISP of this type of surface increased from 18% to 35% (Fig. 3b), indicating extensive regular urbanization in Guangzhou. This regular urbanization was mainly driven by typical urban expansion, with a large amount of rural land, e.g., farmland (Fig. 3a9), bare land (Fig. 3a10 & a11), and forest (Fig. 3a12), being transformed into impervious surfaces. Such changes are closely related to the planning of local economic and technological development zones, as well as the construction of urban-related infrastructure and facilities [69].

Stable-urbanization surfaces account for 30% of the urbanized pixels and are mainly distributed in the peripheral region of the city center (Ellipse II, Fig. 3a). The annual mean ISP of this urbanization type remained very stable (~55%) throughout the study period, with the magnitude of ISP change less than 1% (Fig. 3b). This accords well with the approximately stable land use and/or land cover change within old urban areas [22,23]. New buildings or roads within stable-urbanization surfaces were barely detected, although land use change (e.g., from vegetation to bare land) is still identifiable (Fig. 3a6). Stable-urbanization surfaces correspond well to: (1) large densely-distributed old buildings within city villages (Fig. 3a5), (2) permanent railway land (Fig. 3a7), and (3) to areas that surround water bodies (Fig. 3a8). The occurrence of stable urbanization over these surfaces is probably a result of the very high cost and difficulty of renewing urban villages [51]. The requirement for preserving public facilities and ecological land may also be a cause of the emergence of stable urbanization.

Counter-urbanization surfaces account for the smallest proportion (8%) of the urbanized areas and they are mostly concentrated in the city center (Ellipse III, Fig. 3a). During the study period, its annual mean ISP decreased very significantly, from 71% to 55% (Fig. 3b). Counter urbanization results mainly from typical urban renewal and/or greening activities, such as park construction (Fig. 3a1), street and community greening (Fig. 3a2 & a4), and the conversion from old buildings to vegetation (Fig. 3a3). These greening and renewal activities have resulted in a significant increase in vegetation cover in the city center. Counter urbanization caused by urban renewal activities are also observable in several other cities, e.g., Shanghai in China [46], and Lyon in France [20].

4.2. Spatiotemporal SUHII variations for different urbanization types

For each urbanization type, we analyzed the annual mean and spatial variations of SUHII, both during the day and at night (Figs. 4 and 5). The results show that, for all the three urbanization types, the annual mean SUHII shows an increasing trend during daytime but an insignificant trend at night (Fig. 4a and b). The notable increasing trend in daytime SUHII for regular urbanization is understandable given the associated substantial increase in ISP. By contrast, for the counter- and stable-urbanization surfaces where the ISP has even decreased substantially or remains unchanged, trends of increasing SUHII similar to that for regular-urbanization surfaces are evident. Specially, the SUHII trend for counter-urbanization surfaces (i.e., the city center) is smaller than that for stable-urbanization surfaces (i.e., areas surrounding the city center). These trends in Guangzhou differ from the recent similar cases in Beijing, which despite experiencing counter urbanization showed a decreasing SUHII trend in the city center [47]. This contrast indicates the possibility of a very different daytime SUHII trend over city centers, even for cities undergoing a similar counter-urbanization process. Further explanation of this phenomenon is given in Section 4.3.1.

At night, the annual mean SUHII variations for all three urbanization types show an insignificant decreasing trend ($0.24 \leq p \leq 0.26$) (Fig. 4b), in spite of the prevalent ISP increase for regular-urbanization surfaces. These identified insignificant nighttime SUHII trends over the city center and the surrounding areas are consistent with the results of previous research in Guangzhou [22], although stable- and counter-urbanization surfaces were also separated.

Careful assessment reveals large disparities in SUHII among different urbanization processes (Fig. 4c). The SUHII of counter-urbanization is always greater than those of regular- and stable-urbanization during both daytime and at night. The SUHII of counter urbanization is 7.2 K during the day and 3.4 K at night, while the intensities for the other two urbanization types decrease on average by 2.7 K and 1.3 K during the daytime and at night, respectively. This phenomenon can be attributed to changes in the gradient of the control contribution from the city center to the periphery (Note that the spatial patterns of the contribution from each control are provided in Fig. S3 given in Supplementary Material).

We further analyzed the pixel-based magnitude of change in SUHII for each urbanization process during the study period (Fig. 5). The results reveal a large disparity between daytime and nighttime; during the day, more significant SUHII increase occurs over the city periphery, while the SUHII increase in the city center is more enhanced at night. In other words, during the day, a large growth of SUHII mostly occurs over regular- and stable-urbanization surfaces, whereas they often appear over counter-urbanization surfaces at night. Furthermore, when compared with the daytime case, the pixels with a reduced nighttime SUHII become more concentrated over the regular- and stable-urbanization surfaces located in the northwestern region around the city center (see Ellipse IV in Fig. 5b), whereas those pixels with a large nighttime SUHII growth in the southeastern region are less concentrated (Ellipse VI in Fig. 5b). In addition, when referenced to the daytime case, counter-urbanization pixels around the city center with a large SUHII

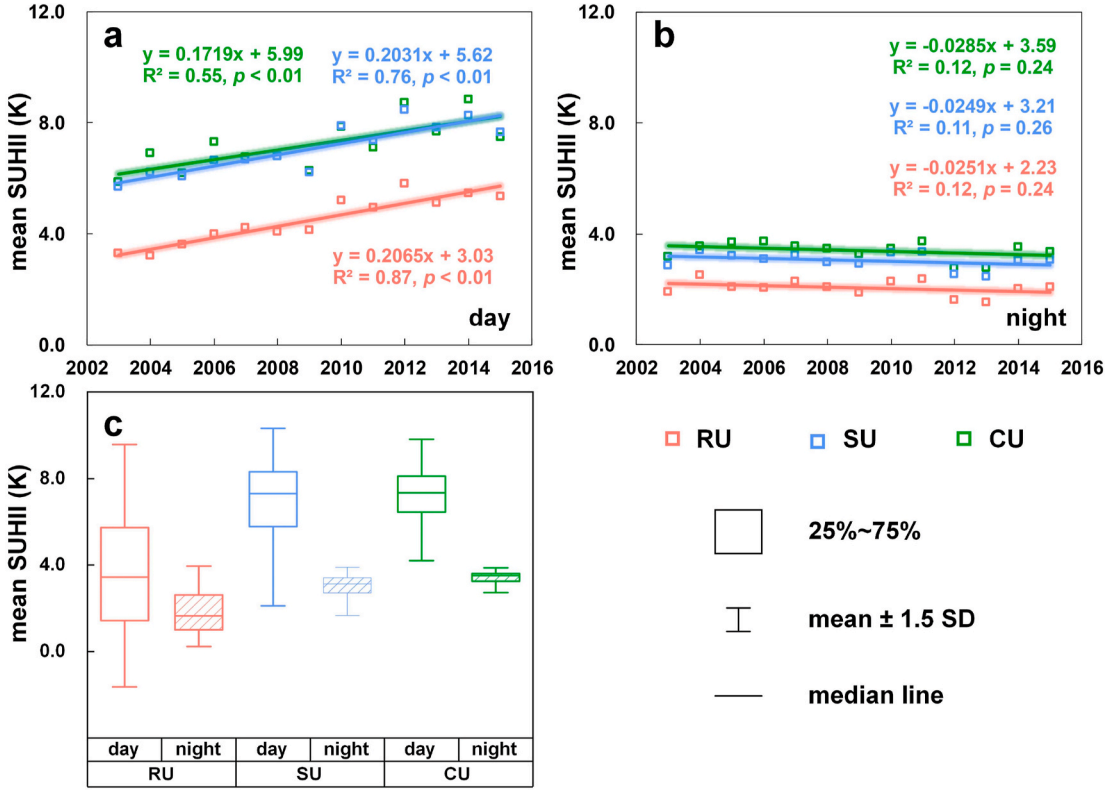

Fig. 4. Annual mean SUHII variations for regular urbanization (RU), stable urbanization (SU), and counter urbanization (CU) during the day (**a**) and at night (**b**), and the pixel-based multi-year (2003–2015) mean SUHII for these three urbanization types (**c**).

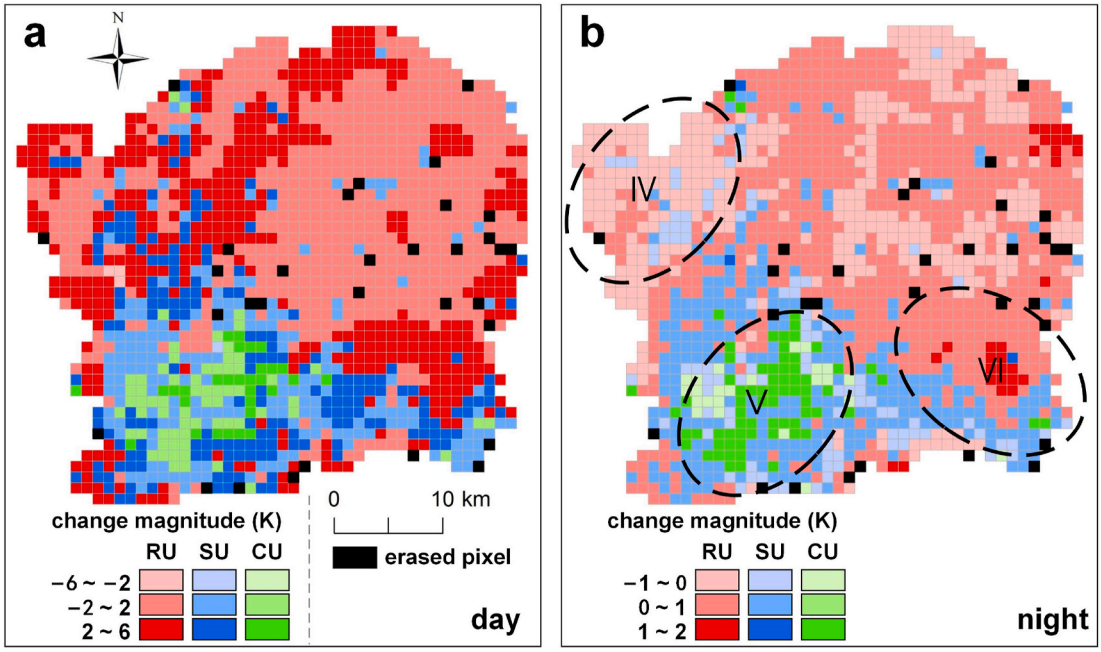

Fig. 5. Spatial distribution of the magnitude of change in daytime SUHII (**a**) and nighttime SUHII (**b**) during the study period for regular urbanization (RU), stable urbanization (SU), and counter urbanization (CU).

growth become more concentrated at night (see Ellipse V in Fig. 5b). The day-night contrast in the spatial distribution of the magnitude of the change in SUHII may be attributed to the spatial distribution of the ISP. The ISP over the city center of Guangzhou (which corresponds well to counter-urbanization surfaces) is significantly larger than that over the city periphery (which corresponds well to regular-urbanization surfaces) [70,71]. This gradient in ISP can lead to a higher concentration of major SUHII growth over counter-urbanization surfaces (i.e., the city center) during the night than in the day, as nocturnal cooling is more suppressed with a higher ISP (or a lower sky view factor) [30,38].

4.3. Contributions of the controls to inter-annual dynamics of SUHII for different urbanization types

4.3.1. Contributions of controls in daytime

4.3.1.1. Contributions of controls to the inter-annual trend in daytime SUHII. The inter-annual SUHII trends of different urbanization types, as well as the contributions of the associated controls to such trends, are shown in Fig. 6. Considering that the RBL-induced contribution is identical for these three types of urbanization as the rural background is shared for these three urbanization types in the calculation of SUHII [57], we now focus mainly on the similarities and disparities in the contributions from the three other controls: ISP, POD, and REF.

The results show that the contribution of each control differs for the three urbanization processes (Fig. 6). Over regular-urbanization surfaces, the increasing SUHII trend is mainly due to the increase in ISP; both POD and REF contribute substantially to the increasing trend in SUHII over stable-urbanization surfaces, while the combined impact from ISP and REF leads to SUHII variations over counter-urbanization surfaces (Fig. 6).

For regular-urbanization surfaces, the contribution from the ISP to the inter-annual SUHII trend is the greatest (43.6%), but it becomes negligible for stable-urbanization surfaces (<3%), and is significantly negative for counter-urbanization surfaces (−26.6%) (Table 1). The contribution from the ISP over counter-urbanization surfaces is negative due to the decrease in ISP. This also partly explains the slightly smaller SUHII trend for counter urbanization compared with those of the other

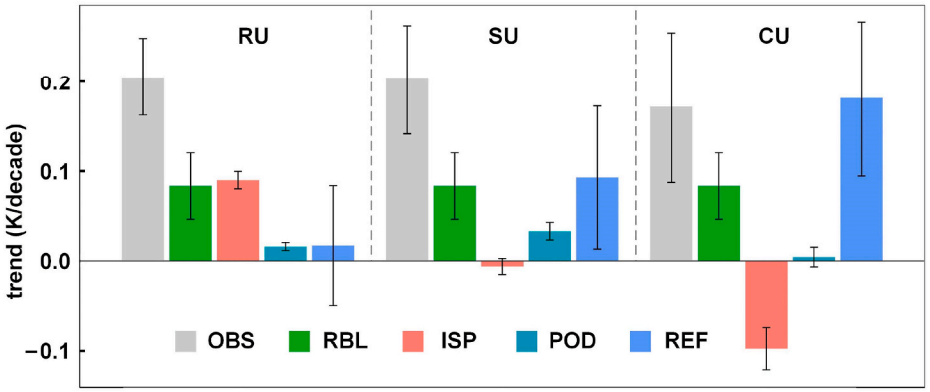

Fig. 6. Contribution of each control to the inter-annual dynamics of daytime SUHII, with the error bars indicating the 5%–95% range of uncertainty. RU, SU, and CU denote regular-, stable-, and counter-urbanization, respectively. OBS denotes the trend in observed SUHII; and RBL, ISP, POD, and REF denote the SUHII trend induced by rural background LST, impervious surface percentage, population density, and residual factors, respectively.

Table 1
Proportional contribution of each control of the inter-annual daytime SUHII dynamics of the three types of urbanization.

Urbanization type	ISP	POD	RBL	REF
Regular urbanization	43.6%	7.8%	40.4%	8.3%
Stable urbanization	−2.9%	15.3%	38.7%	43.1%
Counter urbanization	−26.6%	1.2%	22.7%	49.5%

two types of urbanization (Fig. 4a). The contribution from POD to the inter-annual SUHII trend is relatively small for all three urbanization types, but with a disparity: The contribution reaches a maximum for stable-urbanization surfaces, becomes lower for regular-urbanization surfaces, and becomes minimal for counter-urbanization surfaces (Fig. 6 & Table 1). This disparity corresponds well to the higher growth rate of population density over stable- compared to regular- and counter-urbanization surfaces (see Fig. S4 in Supplementary Material).

The contribution from REF for counter- and stable-urbanization surfaces is greater compared with that for regular-urbanization surfaces (Table 1). This indicates the greater impact of REF over the city center and the surrounding area than over the city periphery. As indicated in Section 3.3, the REF includes a series of factors such as background climate, city size, and urban land cover status, which are now discussed in turn: (1) Background climate change (Fig. S2a in Supplementary Material) is anticipated to have a greater impact on the SUHII over the city center than over the periphery [9,43,72,73]. This is mainly because background climatic change can promote greater energy consumption (induced by increased urban cooling demand during summer) over the city center, where there is a denser population, greater energy consumption, and therefore a higher SUHII [22,24,74,75]. (2) The increase in city size (Fig. S2b in Supplementary Material) due to urban expansion is also expected to have a greater impact on the SUHII of the city center compared with the periphery [72,73]. (3) The more complex urban land cover status over the city center compared with the periphery, which results from a rougher surface and less efficient surface heat release over the city center [15,30,38,44], may also lead to the higher contribution of REF [28,76].

4.3.1.2. Contributions of controls to daytime SUHII during different time intervals. The mean contribution of each control to the absolute SUHII during the three time-intervals of 2003–2005, 2006–2010, and 2011–2015 are shown in Fig. 7. The results show that the SUHII difference among the three types of urbanization surface is regulated more by ISP and REF than by RBL and POD, and that the contributions of these controls vary between time intervals. Specifically, the contributions of ISP and REF are the greatest over the areas close to the city center (i.e., counter-urbanization surfaces), while the contributions of RBL and POD are relatively unchanged or vary only slightly over surfaces with different urbanization processes. In terms of ISP and REF, the contribution from REF gradually increases over regular-urbanization surfaces during the three time-intervals, while that of ISP increases more rapidly. Over stable-urbanization surfaces, however, the contribution of REF increases rapidly, while that of ISP remains relatively constant. Comparatively, the contribution of REF increases rapidly while that of ISP shows a decreasing trend over counter-urbanization surfaces.

4.3.2. Contributions of controls during nighttime

The analysis in Fig. 4b has shown that the nighttime trends in SUHII over all three urbanization types are insignificant ($p < 0.05$). We now further demonstrate the individual contribution of each control to the inter-annual nighttime SUHII trend (Fig. 8). Note that the ISP-induced contribution over stable-urbanization surfaces and the ISP-and POD-induced contributions over counter-urbanization surfaces are not given in Fig. 8 because the statistical relationship is not significant (i.e., $p > 0.05$) for Eq. (4). The results imply that these insignificant trends result from the large uncertainties in the contributions of the controls. For example, the estimated RBL- and REF-induced contributions have large uncertainties, with the error bar exceeding the mean. The ISP-induced contribution is stable only for regular-urbanization surfaces. The uncertainty of the estimated POD-induced contribution remains relatively low and is relatively small compared with those of the other controls.

The large uncertainties in the estimation of the RBL-induced contribution may be derived from the insignificant relationships between nighttime LST and the greening of the rural background (Fig. 9). This differs from the daytime case, for which rural background greening is usually accompanied by stronger surface evapotranspiration cooling under strong solar radiation [9,13]. The weak relationship between RBL and nighttime SUHII was also partly demonstrated in previous reports [22,23]. The estimation of the contribution of the ISP is only uniform over regular-urbanization surfaces, mostly due to higher heat storage release at night caused by the rapid growth of the ISP over such surfaces (Fig. 3). Although the POD maintains a relatively low uncertainty, its absolute contribution is considerably lower than those from the other controls. The stable POD-induced contribution over regular- and stable-urbanization surfaces may be due to the rapid increase in the population density of these areas (see Fig. S4b at Supplementary Material). The greater impact of AHR on SUHIIs during the night than during the day, caused by an increase in population density, may also contribute to the more stable estimate of the POD-induced contribution [23,24].

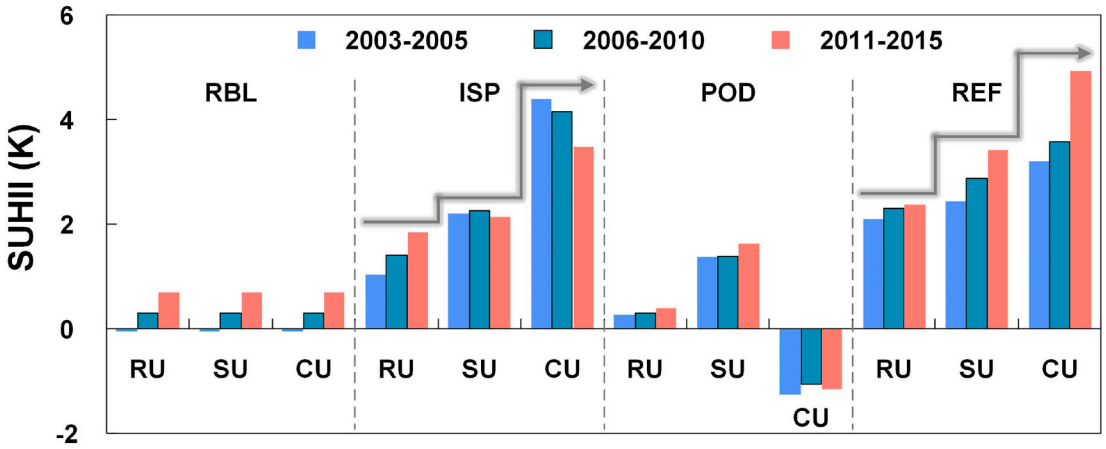

Fig. 7. Mean contribution of each control to the inter-annual daytime SUHII variations for each type of urbanization during the time-intervals of 2003–2005, 2006–2010, and 2011–2015. RU, SU, and CU denote regular-, stable-, and counter-urbanization, respectively. RBL, ISP, POD, and REF denote the SUHII trend induced by rural background LST, impervious surface percentage, population density, and residual factors, respectively.

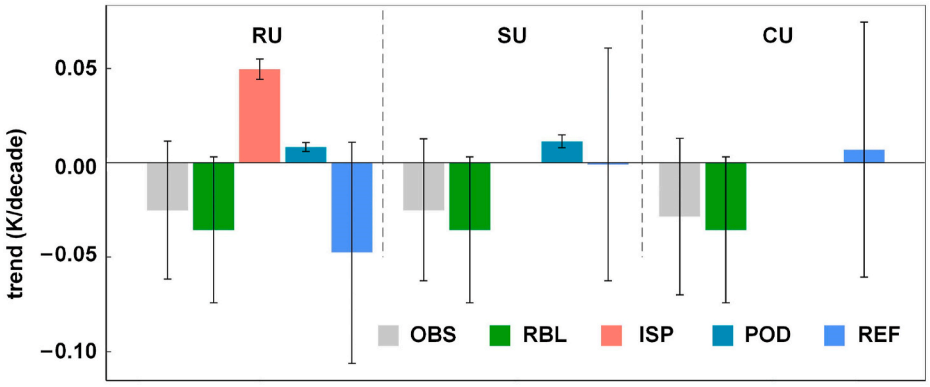

Fig. 8. As Fig. 6, but for the nighttime case.

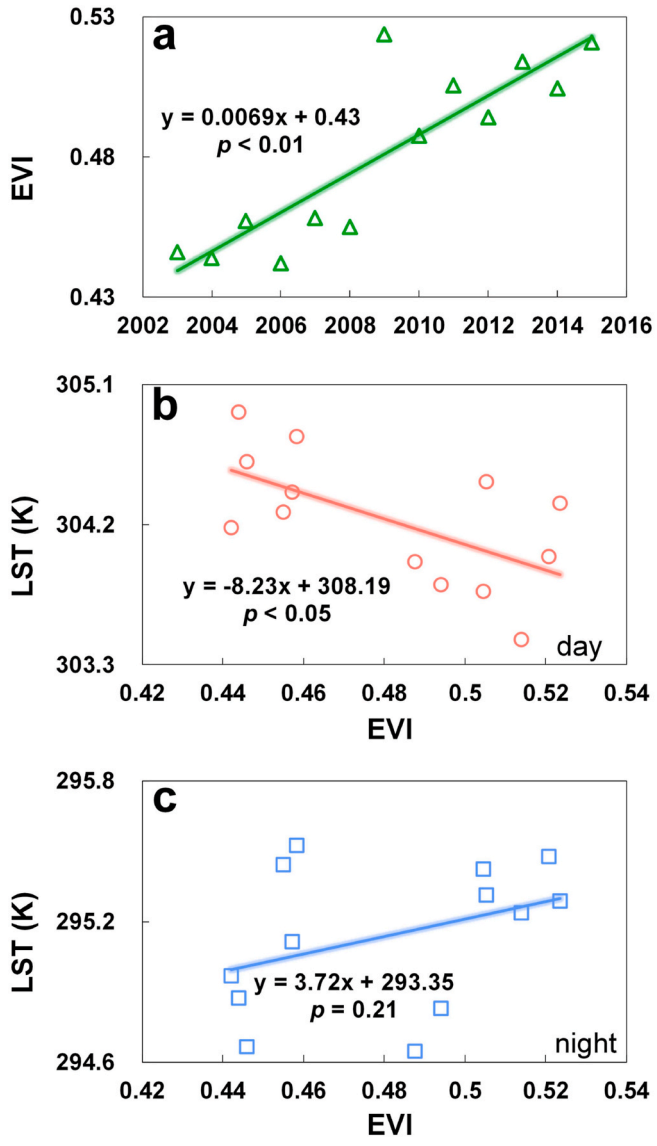

Fig. 9. Change in rural EVI during the study period (**a**) and the relationships between LST and EVI during the day (**b**) and at night (**c**). Subfigure (**a**) shows a significant greening trend in rural background, and subfigure (**b**) shows a significant decreasing trend in the daytime LST of rural background with the increase of rural EVI, while subfigure (**c**) indicates an insignificant relationship between the LST and EVI of rural background.

5. Discussion and implications

5.1. Implications for the design of heat mitigation strategies

For the majority of previous SUHI studies, land use/cover change within cores was usually assumed to be negligible [22,23,34,72], although this assumption will probably bias the estimation of the contributions from various controls to SUHII variations. For instance, urban renewal was recently demonstrated to be able to alter the land use/cover type of the urban cores of several metropolises (e.g., Guangzhou and Shanghai in China and Lyon in France) [20,25,46]. The latest studies have further indicated that such massive urban renewal is even capable of significantly reducing the SUHII in the city center [47]. However, the spatiotemporal patterns of SUHII variations, especially over the city center where there has been massive urban renewal, are still not completely clear. To our best knowledge, our study of the spatiotemporal SUHII variations and their controls in Guangzhou serves as the first to be conducted from the perspective of urbanization type.

Mitigation of the SUHI is an important way to improve the livelihoods of urban residents and to promote sustainable development of a city. Our results indicate that there are significant disparities among the local SUHIs over the surfaces that undergo different types of urbanization. We found that although a similar trend of increasing SUHII is observed for all three urbanization types over Guangzhou, the contribution of each control differs substantially (the spatial pattern of the individual impacts of factors see Fig. S3 in Supplementary Material). These imply that different mitigation strategies should be applied to the mitigation of the local SUHIs over surfaces of different types of urbanization to achieve sustainable urban development. For regular-urbanization surfaces, the increasing trend is primarily driven by the increase in the ISP; and special attention should therefore be directed to the city periphery in the initial stage of urban expansion, e.g., through the control management of the sprawl of low-density buildings to maximize the blue-green landscape [32–34]. For counter-urbanization surfaces, the reduction in the ISP due to urban renewal has a significant cooling effect that offsets warming; therefore, urban planning departments should consider not only the economic benefits of urban renewal, but also the eco-environmental benefits, which may be quantified by the heat island mitigation index [77]. Over stable-urbanization surfaces where the land use/cover types remain relatively unchanged, the increasing trend in SUHII is a result of the combination of REF and AHR (Fig. 6). The negative impact due to the increase in AHR (see Fig. S4a in Supplementary Material) can be offset by using energy-saving air-conditioning units and adopting the design of greening roof strategies [78,79].

5.2. Limitations and prospects

Although progress has been made in understanding the inter-annual variations and controls of the SUHI over Guangzhou, the following issues need to be addressed in future studies.

In terms of data, satellite images of Guangzhou suffer from cloud contamination [54]. This issue was addressed by the temporal aggregation of dense MODIS LSTs obtained under the clear-sky condition, but two shortcomings remain. (1) This current study mainly focuses on the mean local SUHII for each urbanization type and therefore does not require LST data with a high spatial resolution. For the investigation of local SUHI at a finer scale, this shortcoming may be overcome by the fusion of LST data from multiple sources, such as MODIS and Landsat LSTs [80]. (2) Satellite-derived clear-sky LST products may not be suitable for investigating SUHIs under overcast conditions. This shortcoming may be addressed by incorporating reconstruction methods capable of estimating under-cloud LSTs [81]. (3) The thresholds for true changes over urban surfaces may depend on the economic development level, topography, land cover, and other factors of the specific city, which are usually not easy to obtain. The thresholds used in this study over a single city (i.e., Guangzhou) were set based on sub-pixel impervious surface data, while a more universal approach applied for determining the thresholds of true urban changes over a large number of cities with different surface status remain necessary [1]. (4) Although the coordinate system and spatial resolution of multi-source data have been unified, there may still be geographic deviations among these data from multiple sources. Therefore, more effective methods are required to mitigate the impact of geographic deviations of various data for the analysis, especially for studies at a spatial scale much finer than 1 km.

In terms of methodology, the following issues should be addressed. (1) Collinearity among controls. Although the ISP and POD are widely used for representing urban land use/cover and AHR in both local and global studies [6,39,82], there may be collinearity between these two surface parameters. More advanced approaches that can overcome this issue may be used in the future [8,21]. (2) Separation of the individual contribution of controls summarized as REF. Controls such as background climate change and city size have been combined as REF. *In-situ* surface air temperatures and precipitation may be used to help separate the contribution from background climate change [23,24]; however, there are usually an inadequate number of stations to cover all three urbanization types. Future studies may consider the incorporation of urban climate models to separate the individual contributions of these REF-related controls. (3) Different urbanization processes induce many changes in other various physical factors in addition to the controls such as the land cover. The impacts of changes in economic activities, transportation systems, infrastructure, and other physical aspects on local SUHI under different urbanization processes should be further incorporated.

6. Conclusions

Various urbanization processes within cities can result in different spatiotemporal SUHII variations. Using Guangzhou in China as an example, we have attempted to identify all three urbanization types (i.e., regular-, stable-, and counter-urbanization), and to investigate simultaneously the inter-annual SUHII dynamics and the associated controls over surfaces with all three types of urbanization process.

Our results show that the spatial distribution of the three urbanization types exhibits a concentric circle structure. The mean ISP of regular-urbanization surfaces increased by 17% during the study period. The mean ISP of counter-urbanization surface also changed by a similar percentage (i.e., 16%), but it shows a decreasing rather than an increasing trend, indicating the significant impact of urban renewal over the city center. For the stable-urbanization surface, the mean ISP changed by less than 1%.

Our findings reveal disparities and similarities in the SUHI variations responsive to regular-, stable-, and counter-urbanization. The absolute SUHIIs over these three urbanization types are quite different. The SUHII over regular-urbanization surfaces is lower than that over stable-urbanization surfaces, and even lower than that over counter-urbanization surfaces. However, the inter-annual SUHII trends of the three urbanization types are similar – they are all characterized by a significant daytime increase (greater than 0.17 K decade^{-1}), while there is an insignificant trend at night.

For the SUHII controls, over all the three urbanization types the RBL-induced contributions to the SUHII dynamics are identical, and ISP and REF are shown to be two important controls. However, the dominant controls that regulate the inter-annual SUHII variations differ among the three urbanization types. Over regular-urbanization surfaces, ISP is the major control of the increasing SUHII trend, with a contribution up to 43.6%; POD and REF are the two dominant controls over stable-urbanization surfaces, together contributing 58.4% to the SUHII trend; and the reduction of ISP and REF contribute −26.6% and 49.5%, respectively, to the inter-annual SUHII variations over counter-urbanization surfaces.

These findings contribute to an in-depth understanding of the spatiotemporal SUHI variations in the context of cities that experience various urbanization processes concurrently.

Declaration of competing interest

The authors declare that they have no known competing financial interests or personal relationships that could have appeared to influence the work reported in this paper.

Acknowledgments

This work was jointly supported by the National Key R&D Program of China under Grant number 2017YFA0603604, the Fundamental Research Funds for the Central Universities under Grant number 090414380024, the Jiangsu Provincial Natural Science Foundation under Grant number BK20180009, the National Natural Science Foundation of China under Grant number 41671420, and the National Youth Talent Support Program of China.

Appendix A. Supplementary data

Supplementary data related to this article can be found at https://doi.org/10.1016/j.buildenv.2021.107935.

References

[1] Q. Weng, Remote sensing of impervious surfaces in the urban areas: requirements, methods, and trends, Rem. Sens. Environ. 117 (2012) 34–49, https://doi.org/10.1016/j.rse.2011.02.030.
[2] Z. Zhu, Y. Zhou, K.C. Seto, E.C. Stokes, C. Deng, S.T. Pickett, H. Taubenböck, Understanding an urbanizing planet: strategic directions for remote sensing, Rem. Sens. Environ. 228 (2019) 164–182, https://doi.org/10.1016/j.rse.2019.04.020.
[3] L. Howard, Climate of London deduced from meteorological observation, Harvey and Darton 1 (3) (1833) 1–24.
[4] N. Schwarz, S. Lautenbach, R. Seppelt, Exploring indicators for quantifying surface urban heat islands of European cities with MODIS land surface temperatures, Rem. Sens. Environ. 115 (12) (2011) 3175–3186, https://doi.org/10.1016/j.rse.2011.07.003.
[5] C. Heaviside, H. Macintyre, S. Vardoulakis, The urban heat island: implications for health in a changing environment, Current environmental health reports 4 (3) (2017) 296–305, https://doi.org/10.1007/s40572-017-0150-3.
[6] K. Deilami, M. Kamruzzaman, Y. Liu, Urban heat island effect: a systematic review of spatio-temporal factors, data, methods, and mitigation measures, Int. J. Appl. Earth Obs. Geoinf. 67 (2018) 30–42, https://doi.org/10.1016/j.jag.2017.12.009.
[7] H. Shen, L. Huang, L. Zhang, P. Wu, C. Zeng, Long-term and fine-scale satellite monitoring of the urban heat island effect by the fusion of multi-temporal and multi-sensor remote sensed data: a 26-year case study of the city of Wuhan in China, Rem. Sens. Environ. 172 (2016) 109–125, https://doi.org/10.1016/j.rse.2015.11.005.
[8] D. Zhou, J. Xiao, S. Bonafoni, C. Berger, K. Deilami, Y. Zhou, S. Frolking, R. Yao, Z. Qiao, J.A. Sobrino, Satellite remote sensing of surface urban heat islands:

progress, challenges, and perspectives, Rem. Sens. 11 (1) (2019), https://doi.org/10.3390/rs11010048, 48.
[9] M.L. Imhoff, P. Zhang, R.E. Wolfe, L. Bounoua, Remote sensing of the urban heat island effect across biomes in the continental USA, Rem. Sens. Environ. 114 (3) (2010) 504–513, https://doi.org/10.1016/j.rse.2009.10.008.
[10] Q. Meng, L. Zhang, Z. Sun, F. Meng, L. Wang, Y. Sun, Characterizing spatial and temporal trends of surface urban heat island effect in an urban main built-up area: a 12-year case study in Beijing, China, Rem. Sens. Environ. 204 (2018) 826–837, https://doi.org/10.1016/j.rse.2017.09.019.
[11] K.C. Seto, P. Christensen, Remote sensing science to inform urban climate change mitigation strategies, Urban Climate 3 (2013) 1–6, https://doi.org/10.1016/j.uclim.2013.03.001.
[12] N. Clinton, P. Gong, MODIS detected surface urban heat islands and sinks: global locations and controls, Rem. Sens. Environ. 134 (2013) 294–304, https://doi.org/10.1016/j.rse.2013.03.008.
[13] S. Peng, S. Piao, P. Ciais, P. Friedlingstein, C. Ottle, F.M. Bréon, H. Nan, L. Zhou, R. B. Myneni, Surface urban heat island across 419 global big cities, Environ. Sci. Technol. 46 (2) (2012) 696–703. https://pubs.acs.org/doi/10.1021/es2030438.
[14] R. Yao, L. Wang, X. Huang, W. Gong, X. Xia, Greening in rural areas increases the surface urban heat island intensity, Geophys. Res. Lett. 46 (4) (2019) 2204–2212, https://doi.org/10.1029/2018GL081816.
[15] L. Zhao, X. Lee, R.B. Smith, K. Oleson, Strong contributions of local background climate to urban heat islands, Nature 511 (7508) (2014) 216–219, https://doi.org/10.1038/nature13462.
[16] M. Kim, K. Lee, G.H. Cho, Temporal and spatial variability of urban heat island by geographical location: a case study of Ulsan, Korea, Build. Environ. 126 (2017) 471–482, https://doi.org/10.1016/j.buildenv.2017.10.023.
[17] X. Li, W. Li, A. Middel, S.L. Harlan, A.J. Brazel, Turner Ii, B. L, Remote sensing of the surface urban heat island and land architecture in Phoenix, Arizona: combined effects of land composition and configuration and cadastral–demographic-economic factors, Rem. Sens. Environ. 174 (2016) 233–243, https://doi.org/10.1016/j.rse.2015.12.022.
[18] Y. Lin, C.Y. Jim, J. Deng, Z. Wang, Urbanization effect on spatiotemporal thermal patterns and changes in Hangzhou (China), Build. Environ. 145 (2018) 166–176, https://doi.org/10.1016/j.buildenv.2018.09.020.
[19] J. Peng, J. Jia, Y. Liu, H. Li, J. Wu, Seasonal contrast of the dominant factors for spatial distribution of land surface temperature in urban areas, Rem. Sens. Environ. 215 (2018) 255–267, https://doi.org/10.1016/j.rse.2018.06.010.
[20] F. Renard, L. Alonso, Y. Fitts, A. Hadjiosif, J. Comby, Evaluation of the effect of urban redevelopment on surface urban heat islands, Rem. Sens. 11 (3) (2019) 299, https://doi.org/10.3390/rs11030299.
[21] Z. Li, M. Si, P. Leng, A review of remotely sensed surface urban heat islands from the fresh perspective of comparisons among different regions (invited review), Progress In Electromagnetics Research 102 (2020) 31–46. http://www.jpier.org/pierc/pier.php?paper=20020403.
[22] R. Yao, L. Wang, X. Huang, Z. Niu, F. Liu, Q. Wang, Temporal trends of surface urban heat islands and associated determinants in major Chinese cities, Sci. Total Environ. 609 (2017) 742–754, https://doi.org/10.1016/j.scitotenv.2017.07.217.
[23] R. Yao, L. Wang, X. Huang, W. Zhang, J. Li, Z. Niu, Interannual variations in surface urban heat island intensity and associated drivers in China, J. Environ. Manag. 222 (2018) 86–94, https://doi.org/10.1016/j.jenvman.2018.05.024.
[24] D. Zhou, S. Zhao, S. Liu, L. Zhang, C. Zhu, Surface urban heat island in China's 32 major cities: spatial patterns and drivers, Rem. Sens. Environ. 152 (2014) 51–61, https://doi.org/10.1016/j.rse.2014.05.017.
[25] Y. Fu, J. Li, Q. Weng, Q. Zheng, L. Li, S. Dai, B. Guo, Characterizing the spatial pattern of interannual urban growth by using time series Landsat imagery, Sci. Total Environ. 666 (2019) 274–284, https://doi.org/10.1016/j.scitotenv.2019.02.178.
[26] A.R. Shahtahmassebi, J. Song, Q. Zheng, G.A. Blackburn, K. Wang, L. Huang, Y. Pan, N. Moore, G. Shahtahmassebi, R.S. Haghighi, J. Deng, Remote sensing of impervious surface growth: a framework for quantifying urban expansion and re-densification mechanisms, Int. J. Appl. Earth Obs. Geoinf. 46 (2016) 94–112, https://doi.org/10.1016/j.jag.2015.11.007.
[27] J.P. Connors, C.S. Galletti, W.T. Chow, Landscape configuration and urban heat island effects: assessing the relationship between landscape characteristics and land surface temperature in Phoenix, Arizona, Landsc. Ecol. 28 (2) (2013) 271–283, https://doi.org/10.1007/s10980-012-9833-1.
[28] I. Esau, V. Miles, M. Varentsov, P. Konstantinov, V. Melnikov, Spatial structure and temporal variability of a surface urban heat island in cold continental climate, Theor. Appl. Climatol. 137 (3–4) (2019) 2513–2528, https://doi.org/10.1007/s00704-018-02754-z.
[29] X. Feng, S.W. Myint, Exploring the effect of neighboring land cover pattern on land surface temperature of central building objects, Build. Environ. 95 (2016) 346–354, https://doi.org/10.1016/j.buildenv.2015.09.019.
[30] X. Huang, Y. Wang, Investigating the effects of 3D urban morphology on the surface urban heat island effect in urban functional zones by using high-resolution remote sensing data: a case study of Wuhan, Central China, ISPRS J. Photogrammetry Remote Sens. 152 (2019) 119–131, https://doi.org/10.1016/j.isprsjprs.2019.04.010.
[31] J.S. Silva, R.M. da Silva, C.A.G. Santos, Spatiotemporal impact of land use/land cover changes on urban heat islands: a case study of Paço do Lumiar, Brazil, Build. Environ. 136 (2018) 279–292, https://doi.org/10.1016/j.buildenv.2018.03.041.
[32] R. Sun, Y. Lü, L. Chen, L. Yang, A. Chen, Assessing the stability of interannual temperatures for different urban functional zones, Build. Environ. 65 (2013) 90–98, https://doi.org/10.1016/j.buildenv.2013.04.001.
[33] Z. Xue, G. Hou, Z. Zhang, X. Lyu, M. Jiang, Y. Zou, X. Shen, J. Wang, X. Liu, Quantifying the cooling-effects of urban and peri-urban wetlands using remote sensing data: case study of cities of Northeast China, Landsc. Urban Plann. 182 (2019) 92–100, https://doi.org/10.1016/j.landurbplan.2018.10.015.
[34] J. Wang, W. Zhou, J. Wang, Time-series analysis reveals intensified urban heat island effects but without significant urban warming, Rem. Sens. 11 (19) (2019) 2229, https://doi.org/10.3390/rs11192229.
[35] P. Gong, X. Li, J. Wang, Y. Bai, B. Chen, T. Hu, X. Liu, B. Xu, J. Yang, W. Zhang, Y. Zhou, Annual maps of global artificial impervious area (GAIA) between 1985 and 2018, Rem. Sens. Environ. 236 (111510) (2020), https://doi.org/10.1016/j.rse.2019.111510.
[36] X.P. Song, J.O. Sexton, C. Huang, S. Channan, J.R. Townshend, Characterizing the magnitude, timing and duration of urban growth from time series of Landsat-based estimates of impervious cover, Rem. Sens. Environ. 175 (2016) 1–13, https://doi.org/10.1016/j.rse.2015.12.027.
[37] L. Sun, J. Chen, Q. Li, D. Huang, Dramatic uneven urbanization of large cities throughout the world in recent decades, Nat. Commun. 11 (1) (2020) 1–9, https://doi.org/10.1038/s41467-020-19158-1.
[38] E. Jamei, P. Rajagopalan, M. Seyedmahmoudian, Y. Jamei, Review on the impact of urban geometry and pedestrian level greening on outdoor thermal comfort, Renew. Sustain. Energy Rev. 54 (2016) 1002–1017, https://doi.org/10.1016/j.rser.2015.10.104.
[39] D.J. Sailor, M. Georgescu, J.M. Milne, M.A. Hart, Development of a national anthropogenic heating database with an extrapolation for international cities, Atmos. Environ. 118 (2015) 7–18, https://doi.org/10.1016/j.atmosenv.2015.07.016.
[40] D.J. Sailor, L. Lu, A top–down methodology for developing diurnal and seasonal anthropogenic heating profiles for urban areas, Atmos. Environ. 38 (17) (2004) 2737–2748, https://doi.org/10.1016/j.atmosenv.2004.01.034.
[41] S. Piao, X. Wang, T. Park, C. Chen, X. Lian, Y. He, J.W. Bjerke, A. Chen, P. Ciais, H. Tømmervik, R.R. Nemani, R.B. Myneni, Characteristics, drivers and feedbacks of global greening, Nature Reviews Earth & Environment 1 (1) (2020) 14–27, https://doi.org/10.1038/s43017-019-0001-x.
[42] W. Yue, J. Xu, J. Wu, L. Xu, Remote sensing of spatial patterns of urban renewal using linear spectral mixture analysis: a case of central urban area of Shanghai (1997–2000), Chin. Sci. Bull. 51 (8) (2006) 977–986, https://doi.org/10.1007/s11434-006-0977-8.
[43] S. Chapman, J.E. Watson, A. Salazar, M. Thatcher, C.A. McAlpine, The impact of urbanization and climate change on urban temperatures: a systematic review, Landsc. Ecol. 32 (10) (2017) 1921–1935, https://doi.org/10.1007/s10980-017-0561-4.
[44] L. Yang, D. Niyogi, M. Tewari, D. Aliaga, F. Chen, F. Tian, G. Ni, Contrasting impacts of urban forms on the future thermal environment: example of Beijing metropolitan area, Environ. Res. Lett. 11 (3) (2016), 034018, https://doi.org/10.1088/1748-9326/11/3/034018.
[45] C. Xia, A. Zhang, A.G.O. Yeh, Shape-weighted landscape evolution index: an improved approach for simultaneously analyzing urban land expansion and redevelopment, J. Clean. Prod. 118836 (2019), https://doi.org/10.1016/j.jclepro.2019.118836.
[46] Q. Zhong, J. Ma, B. Zhao, X. Wang, J. Zong, X. Xiao, Assessing spatial-temporal dynamics of urban expansion, vegetation greenness and photosynthesis in megacity Shanghai, China during 2000–2016, Rem. Sens. Environ. 233 (111374) (2019), https://doi.org/10.1016/j.rse.2019.111374.
[47] X. Liu, Y. Zhou, W. Yue, X. Li, Y. Liu, D. Lu, Spatiotemporal patterns of summer urban heat island in Beijing, China using an improved land surface temperature, J. Clean. Prod. 120529 (2020), https://doi.org/10.1016/j.jclepro.2020.120529.
[48] Z. Jiang, W. Zhai, X. Meng, Y. Long, Identifying shrinking cities with NPP-VIIRS nightlight data in China, J. Urban Plann. Dev. 146 (4) (2020), 04020034. https://doi.org/10.1061/(ASCE)UP.1943-5444.0000598.
[49] Guangzhou Statistics Yearbook, Guangzhou statistics Bureau, Retrieved from, http://tjj.gz.gov.cn/, 2018.
[50] J. Xu, Y. Zhao, K. Zhong, F. Zhang, X. Liu, C. Sun, Measuring spatio-temporal dynamics of impervious surface in Guangzhou, China, from 1988 to 2015, using time-series Landsat imagery, Sci. Total Environ. 627 (2018) 264–281, https://doi.org/10.1016/j.scitotenv.2018.01.155.
[51] X. Li, E.C. Hui, T. Chen, W. Lang, Y. Guo, From Habitat III to the new urbanization agenda in China: seeing through the practices of the "three old renewals" in Guangzhou, Land Use Pol. 81 (2019) 513–522, https://doi.org/10.1016/j.landusepol.2018.11.021.
[52] P. Fu, Q. Weng, Variability in interannual temperature cycle in the urban areas of the United States as revealed by MODIS imagery, ISPRS J. Photogrammetry Remote Sens. 146 (2018) 65–73, https://doi.org/10.1016/j.isprsjprs.2018.09.003.
[53] J.O. Sexton, X. Song, C. Huang, S. Channan, M.E. Baker, J.R. Townshend, Urban growth of the Washington, DC–Baltimore, MD metropolitan region from 1984 to 2010 by interannual, Landsat-based estimates of impervious cover, Rem. Sens. Environ. 129 (2013) 42–53, https://doi.org/10.1016/j.rse.2012.10.025.
[54] Z. Zhu, Y. Fu, C.E. Woodcock, P. Olofsson, J.E. Vogelmann, C. Holden, M. Wang, S. Dai, Y. Yu, Including land cover change in analysis of greenness trends using all available Landsat 5, 7, and 8 images: a case study from Guangzhou, China (2000–2014), Rem. Sens. Environ. 185 (2016) 243–257, https://doi.org/10.1016/j.rse.2016.03.036.
[55] R. Sun, W. Xie, L. Chen, A landscape connectivity model to quantify contributions of heat sources and sinks in urban regions, Landsc. Urban Plann. 178 (2018) 43–50, https://doi.org/10.1016/j.landurbplan.2018.05.015.

[56] J. Zhao, X. Zhao, S. Liang, T. Zhou, X. Du, P. Xu, D. Wu, Assessing the thermal contributions of urban land cover types, Landsc. Urban Plann. 204 (103927) (2020), https://doi.org/10.1016/j.landurbplan.2020.103927.
[57] D. Zhou, S. Bonafoni, L. Zhang, R. Wang, Remote sensing of the urban heat island effect in a highly populated urban agglomeration area in East China, Sci. Total Environ. 628 (2018) 415–429, https://doi.org/10.1016/j.scitotenv.2018.02.074.
[58] H. Du, D. Wang, Y. Wang, X. Zhao, F. Qin, H. Jiang, Y. Cai, Influences of land cover types, meteorological conditions, anthropogenic heat and urban area on surface urban heat island in the Yangtze River Delta Urban Agglomeration, Sci. Total Environ. 571 (2016) 461–470, https://doi.org/10.1016/j.scitotenv.2016.07.012.
[59] P. Fu, Q. Weng, A time series analysis of urbanization induced land use and land cover change and its impact on land surface temperature with Landsat imagery, Rem. Sens. Environ. 175 (2016) 205–214, https://doi.org/10.1016/j.rse.2015.12.040.
[60] Y. Wang, Y. Bao, Study on the methods of land use dynamic change research, Prog. Geogr. 18 (81) (1999) 81–87, https://doi.org/10.11820/dlkxjz.1999.01.012 (in Chinese).
[61] X. Li, Y. Zhou, G.R. Asrar, M. Imhoff, X. Li, The surface urban heat island response to urban expansion: a panel analysis for the conterminous United States, Sci. Total Environ. 605 (2017) 426–435.
[62] R. Tang, X. Zhao, T. Zhou, B. Jiang, D. Wu, B. Tang, Assessing the impacts of urbanization on albedo in Jing-Jin-Ji Region of China, Rem. Sens. 10 (7) (2018) 1096, https://doi.org/10.3390/rs10071096.
[63] J. Song, Z.H. Wang, Impacts of mesic and xeric urban vegetation on outdoor thermal comfort and microclimate in Phoenix, AZ. Building and Environment 94 (2015) 558–568, https://doi.org/10.1016/j.buildenv.2015.10.016.
[64] S. Wiesner, B. Bechtel, J. Fischereit, V. Gruetzun, P. Hoffmann, B. Leitl, D. Rechid, K.H. Schlünzen, S. Thomsen, Is it possible to distinguish global and regional climate change from urban land cover induced signals? A mid-latitude city example, Urban Science 2 (1) (2018) 12, https://doi.org/10.3390/urbansci2010012.
[65] S.T. Pickett, Space-for-time substitution as an alternative to long-term studies, in: Long-term Studies in Ecology, Springer, New York, NY, 1989, pp. 110–135, https://doi.org/10.1007/978-1-4615-7358-6_5.
[66] S. Wu, Z. Liang, S. Li, Relationships between urban development level and urban vegetation states: a global perspective, Urban For. Urban Green. 38 (2019) 215–222, https://doi.org/10.1016/j.ufug.2018.12.010.
[67] Y. Cui, X. Xu, J. Dong, Y. Qin, Influence of urbanization factors on surface urban heat island intensity: a comparison of countries at different developmental phases, Sustainability 8 (8) (2016) 706, https://doi.org/10.3390/su8080706.
[68] V. Miles, I. Esau, Surface urban heat islands in 57 cities across different climates in northern Fennoscandia, Urban Climate 31 (100575) (2020), https://doi.org/10.1016/j.uclim.2019.100575.
[69] X. Cui, S. Li, X. Wang, X. Xue, Driving factors of urban land growth in Guangzhou and its implications for sustainable development, Front. Earth Sci. 13 (3) (2019) 464–477, https://doi.org/10.1007/s11707-018-0692-1.
[70] A. Lemonsu, V. Viguié, M. Daniel, V. Masson, Vulnerability to heat waves: Impact of urban expansion scenarios on urban heat island and heat stress in Paris (France), Urban Clim. 14 (2015) 586–605, https://doi.org/10.1016/j.uclim.2015.10.007.
[71] H. Li, Y. Zhou, X. Li, L. Meng, X. Wang, S. Wu, S. Sodoudi, A new method to quantify surface urban heat island intensity, Sci. Total Environ. 624 (2018) 262–272, https://doi.org/10.1016/j.scitotenv.2017.11.360.
[72] A. Lemonsu, V. Viguié, M. Daniel, V. Masson, Vulnerability to heat waves: impact of urban expansion scenarios on urban heat island and heat stress in Paris (France), Urban Climate 14 (2015) 586–605, https://doi.org/10.1016/j.uclim.2015.10.007.
[73] J. Peng, J. Ma, Q. Liu, Y. Liu, Y. Hu, Y. Li, Y. Yue, Spatial-temporal change of land surface temperature across 285 cities in China: an urban-rural contrast perspective, Sci. Total Environ. 635 (2018) 487–497, https://doi.org/10.1016/j.scitotenv.2018.04.105.
[74] D.J. Sailor, C. Vasireddy, Correcting aggregate energy consumption data to account for variability in local weather, Environ. Model. Software 21 (5) (2006) 733–738, https://doi.org/10.1016/j.envsoft.2005.08.001.
[75] J. Yang, Z.H. Wang, K.E. Kaloush, H. Dylla, Effect of pavement thermal properties on mitigating urban heat islands: a multi-scale modeling case study in Phoenix, Build. Environ. 108 (2016) 110–121, https://doi.org/10.1016/j.buildenv.2016.08.021.
[76] Z. Qiao, X. Han, C. Wu, L. Liu, X. Xu, Z. Sun, W. Sun, Q. Cao, L. Li, Scale effects of the relationships between 3D building morphology and urban heat island: a case study of provincial capital cities of mainland China, Complexity 9326793 (2020), https://doi.org/10.1155/2020/9326793.
[77] H. Xu, F. Ding, X. Wen, Urban expansion and heat island dynamics in the Quanzhou region, China, IEEE Journal of selected topics in applied earth observations and remote sensing 2 (2) (2009) 74–79, https://doi.org/10.1109/JSTARS.2009.2023088.
[78] P.A. Mirzaei, Recent challenges in modeling of urban heat island, Sustainable Cities and Society 19 (2015) 200–206, https://doi.org/10.1016/j.scs.2015.04.001.
[79] R. Pacheco, J. Ordóñez, G. Martínez, Energy efficient design of building: a review, Renew. Sustain. Energy Rev. 16 (6) (2012) 3559–3573, https://doi.org/10.1016/j.rser.2012.03.045.
[80] Q. Weng, P. Fu, F. Gao, Generating daily land surface temperature at Landsat resolution by fusing Landsat and MODIS data, Rem. Sens. Environ. 145 (2014) 55–67, https://doi.org/10.1016/j.rse.2014.02.003.
[81] P. Fu, Y. Xie, Q. Weng, S. Myint, K. Meacham-Hensold, C. Bernacchi, A physical model-based method for retrieving urban land surface temperatures under cloudy conditions, Rem. Sens. Environ. 230 (111191) (2019), https://doi.org/10.1016/j.rse.2019.05.010.
[82] M.G. Flanner, Integrating anthropogenic heat flux with global climate models, Geophys. Res. Lett. 36 (L02801) (2009), https://doi.org/10.1029/2008GL036465.